WOOD RESEARCH
60 (6): 2015
857-864

ANALYSIS OF WOOD PORE CHARACTERISTICS WITH MERCURY INTRUSION POROSIMETRY AND X-RAY MICRO- COMPUTED TOMOGRAPHY

Li Min Peng, Dong Wang, Feng Fu, Bo Qi Song
Research Institute of Wood Industry
Chinese Academy of Forestry
Beijing
China

(Received April 2015)

ABSTRACT

The size and distribution of wood pores greatly influence its properties like density, thermal conductivity and permeability as well as acoustical property. Different techniques were developed to measure wood pore characteristic parameters. In this paper, mercury intrusion porosimetry (MIP) and X-ray Micro-computed tomography (μCT) were used to characterize pore characteristics of *Populus* L. woods. Pore size distribution and total porosity results were achieved. As for MIP measurement, the pore size of *Populus* L. woods ranged from 50 to 400 μm. The pore volume in the range of 313-2513.7 nm and 8-400 μm for 0.23 $g.cm^{-3}$ sample was significantly larger than that of 0.40 $g.cm^{-3}$ sample, but the pore volume in the range of 2513.7-7878 nm was less. And the pore distribution tendency for μCT measurement between 2.84~36.86 μm was similar with MIP. According to the results of μCT and intrusion–extrusion curves hysteresis regions of MIP, the existence of ink-bottle effect of MIP was confirmed. So the MIP measured pore-size distribution of micro-voids was larger than actual value.

KEYWORDS: Mercury intrusion porosimetry, X-ray micro-computed tomography, pore size distribution, ink-bottle effect.

INTRODUCTION

As a natural porous material, wood is composed of vertical array of cells and horizontal ray cells. These cells, which are mainly connected by the pits and other micro-voids, formed many macro-voids. Those voids characteristics determine many wood properties, particularly density, thermal conductivity, permeability and acoustical property. For example, the wood porosity is a dominant influence factor in air permeability, impregnation rate and polymer retention (Suleiman et al. 1999, Ding et al. 2008).

It has important implication for wood properties research that how to accurately measure pore characteristics. The MIP is one of the most commonly used method to characterize wood pore size and distribution because of its simple operation and good stability. It forces mercury into pores with the help of pressure, the pore volume is determined by the entered pore mercury volume, and pore size is determined by the pressure needed. Plötle and Niemz (2011) studied the porossity, pore size, distribution, and specific surface area of different wood species with MIP method. It was reported that the total specific surface area value by MIP was lower than the value by the water vapour adsorption technique (Plötze and Niemz 2011). Wang (2014) and He et al. (2014) utilized MIP method to study the mechanism of permeability improvement of microwave treated wood by compared with the changes in pore characteristics before and after treatment. MIP was also used to evaluate the impregnation mechanisms of wood by methyl methacrylate (MMA) through examining the changes in porosity, pore volume, pore size distribution and bulk density of solid wood before and after MMA impregnation (Moro and Bőhni 2002).

However, the MIP method in measuring pore size and distribution has its limitations. The most significant limitation is the ink-bottle effect. Wood is composed of hollow cells which are mainly connected by pits and tiny voids. Those pits and tiny voids are main channels of air and liquid circulation between adjacent cells. Considering a geometry of wood cell with successively cell lumen and pit, cell lumen will only get filled with mercury at the Kelvin-Laplace intrusion pressure of the pits and tiny voids (Young 1805). This leads to an overestimation of the pits and tiny voids volume and an underestimation of the cell lumen volume (Roels et al. 2001, Moro and Bőhni 2002). Moreover, those ink-bottle pores influenced contact angle of mercury against cell wall (Penumadu and Dean 2000).

In order to understand limitations of MIP for wood pore measurement, X-ray micro-computed tomography (μCT) had been employed. The μCT could be used to visualize the inner structure of a material or biological tissue in a non-destructive and visual manner. Previous studies reported the applications of μCT to study the dendrochronology of wood and to identify wood species (Mizuno et al. 2010, Moore et al. 2004, Steppe et al. 2004). The analysis of images provided by μCT allowed the quantitative assessment of scaffold void fraction and accessible void fractions at increasing connection sizes, and computer-assisted analysis of μCT images exhibited a potential for the quantitative analysis of porous scaffold interconnectivity (Moore et al. 2004). Cnudde et al. (2009) examined the porosity and microstructure characterization of construction stones and concretes with μCT and MIP. Pore size distribution curves ranging 10 nm to 1 mm and total porosity were obtained. Both μCT and MIP were compared in respective of their advantages and disadvantages.

The main objective of this research was to analyze the limitations of MIP for measurement wood pores characteristics, and μCT as a new non-destructive method was put forward to characterize wood porosity, pore size and distribution. The μCT and MIP for measurement wood pores characteristics were compared and analyzed disadvantages of MIP for measurement wood pore characteristics.

MATERIAL AND METHODS

Materials

The two *Populus* L. logs were collected from Xunyi County of Shaanxi province, China. Their diameters were 15 and 21 cm, and 2.14 and 1.90 m in length, their average air-dried densities were 0.23 and 0.40 g.cm^{-3} respectively. A disc (Φ=15 mm, thickness was 10 mm) was

taken from the middle of each log. For each disc, the MIP sample (5×5×10 mm, radial ×tangential ×longitudinal) and the μCT sample (2×2×10 mm, radial ×tangential ×longitudinal) were cut at the place 4 cm from disc central position and the two samples were adjacent. The samples were dried in an oven at 103±2°C for 24 hours to oven dry moisture content.

Methods

Mercury intrusion porosimetry (MIP)

The MIP characterizing process employed an AutoporeTM IV 9500 Automated Mercury Porosimeter (Micromeritics Instrument Corp., US), to force mercury into pores of wood samples with high pressure (maximum pressure was 400GPa). Measurements of total intrusion volume, total pore surface area, pore size and distribution were all available. The weights of two samples were 0.014 and 0.022 g, respectively. The rate of pressure increase was automatically controlled by the pre-defined procedure, with lower rates at lower pressure levels during measured intrusion processes. As pressure increased, mercury was intruded into voids of descending size and the rate of pressure decreased. The pore volume could be derived from the quantity of mercury intruded. The pore distribution was determined with the Washburn equation (Suleiman et al. 1999).

X-ray micro-tomography scanning (μCT)

A Skyscan 1172 μCT (Bruker Co., Ltd., Germany) with 0.5 μm micron pixel size was used to analyze pore size and distribution and porosity of *Populus* L. woods. First, the sample was fixed on the cylindrical bench (Φ = 4 mm) which rotated between the fixed X-ray source and detector. Second, the sample was positioned then the source generated a polychromatic spectrum where the X-ray intensity was a function of the photon energy. The spectrum depended on the acquisition parameters, namely, voltage, current, and the applied filter material. The polychromatic X-ray was attenuated when passing through samples. The intensity of the attenuated X-ray was measured by the detector, gray-level images representing the attenuation degree were reconstructed. The represented the minimum and maximum intensity. Third, the computer-processed X-rays produced two-dimensional tomographic images which gray levels range from 15 to 225 (Fig. 1).

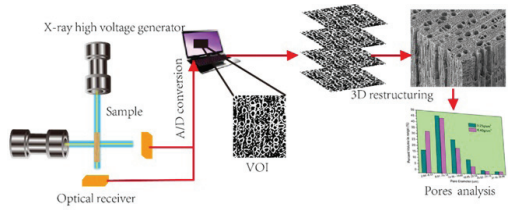

Fig. 1: X-ray micro-tomography scanning and 3D-analysis.

Digital geometry processing was used to generate a three-dimensional image of the inside of a sample from a large series of two-dimensional radiographic images taken around a single axis of rotation (Fig. 1 3D restructuring).

Open porosity analysis methodology (http: // www.doc88.com/p-4971074126021.html. pdf. October 15.2014).

Specialized software (CTAn) was used to analyze Micro-CT 3D images including pore size and distribution, porosity, connectivity. This "CT-3D analysis" included the following two parts:

Part I: The first thing to do after reconstructing a dataset of each sample was to load it onto

the Data Viewer and check the dataset. Then the volume of interest (VOI) was selected (Fig. 1 VOI). This made it easier for CTAn to perform analysis steps and therefore the work could be done more quickly and efficiently. First, only a particular amount of slices were selected from the dataset and secondly there was the possibility of choosing the region of interest (ROI) on each slice. Selecting a ROI on one slice was sufficient, as CTAn would interpolate this ROI to a VOI using all of the selected slices. After this VOI selection, the VOI was saved as a new dataset and then reloaded into CTAn.

Part II: open porosity analysis methodology. The ROI dataset was reloaded. The next step was to make a binary image. Then despeckle: When analyzing the open porosity of the sample the closed pores need to be removed. This could be achieved by the command "Remove Pores". Finally, the pore size was determined by using a structuring element that approximates the shape of a sphere and filled each pore, processing from the smallest inscribed "sphere", to the largest, which is also known as the maximum opening.

RESULTS AND DISCUSSION

The porosity, pore size and distribution detected by MIP

The results derived from the MIP measurement were shown in Tab.1. The total intrusion volumes were 2.02 and 0.97 $g.cm^{-3}$ for the samples of 0.23 and 0.40 $g.cm^{-3}$ respectively, and indicated that the total pores volume for the former was larger than that of the latter. This conclusion was also demonstrated by porosity result (Tab.1). The median pore diameter and total pore area also indicated that the total of micro-voids for 0.23 $g.cm^{-3}$ sample were more than 0.40 $g.cm^{-3}$ sample.

Tab. 1: The MIP test results of two Populus L. woods.

Density ($g.cm^{-3}$)	Total intrusion volume ($cm^3.g^{-1}$)	Total pore area ($cm^2.g^{-1}$)	Median pore diameter (nm)	Porosity (%)
0.23	2.0200	6.321×10^4	2148.2	63.7253
0.40	0.9741	2.040×10^4	7263.1	39.0011

Fig. 2 displayed the relationship between the pore diameter and the mercury intrusion volume. Fig. 3 was the log differential mercury intrusion volume as a function of the pore diameter. The cumulative pore volume of 0.23 $g.cm^{-3}$ sample was about twice larger than that of 0.40 $g.cm^{-3}$ sample (Fig. 2), and this result was consistent with Tab. 1. For the 0.23 $g.cm^{-3}$ sample, the volume in the range of 313 - 2513.7 nm and 8-400 μm pores were 1.1 and 0.76 $cm^3.g^{-1}$, respectively. They were significantly larger than that of 0.40 sample, but the volume in the range of 2513.7-7878 nm pores were less (Figs. 2 and 3). According to the research of Griffin (1977) and Thygesen et al. (2010), the 313-2513.7 nm micro-voids might be pit membrane voids, pit apertures and other small voids, and the 7-80 μm macro-voids might be lumens of the cells (Griffin 1977, Thygesen et al. 2010).

The MIP measurement results were based to intrusion–extrusion curves. The intrusion curve was used to denote the volume change in the process of pressure increase, and the extrusion curve indicated the volume change with decreasing pressure (Fig. 4).The intrusion–extrusion cycle did not close when the initial pressure was reached, which indicated that some mercury has been permanently entrapped in certain pores. In fact, the path followed by the extrusion curve was not the same as the intrusion path (Hysteresis, Fig. 4). At any given pressure, the volume indicated on the extrusion curve was greater than that on the intrusion curve. For a given volume, the pressure

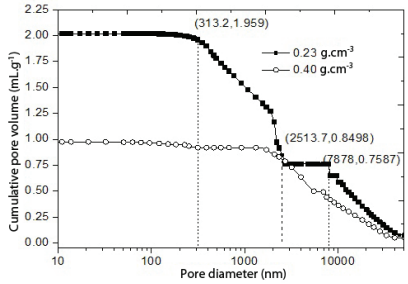

Fig. 2: Cumulative pore volume as a function of the pore diameter of Populus L. *woods.*

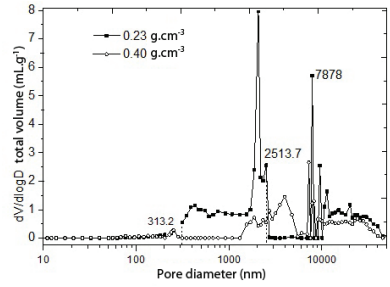

Fig. 3: Log differential intrusion as a function of the pore diameter of Populus L. *woods.*

indicated on the intrusion curve was greater than that on the extrusion curve. Intrusion–extrusion hysteresis and entrapment was attributed to ink-bottle-shaped pores (pit and tiny void). For the 0.23 g.cm^{-3} sample, the micro-voids ranged of 20-1 μm were significantly more than 0.40 g.cm^{-3} samples' (Fig. 2) and resulting in larger hysteresis region (Fig. 4). Cell lumen would only get filled with mercury at the Kelvin-Laplace intrusion pressure of the pits and tiny voids. This led to an overestimation of the pits and tiny voids volume and an underestimation of the cell lumen volume.

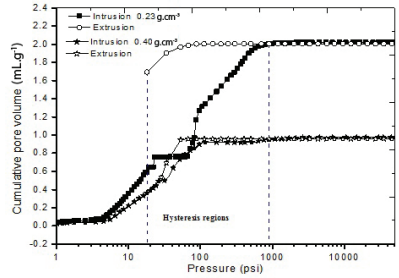

Fig. 4: Cumulative pore volume as a function of the pressure of one intrusion–extrusion cycle.

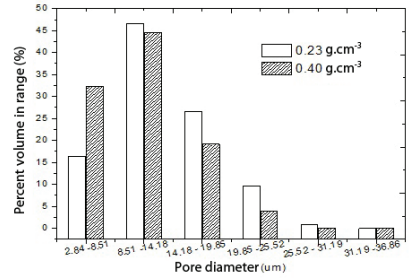

Fig. 5: Open pore diameter distribution of Populus L. *woods by μCT.*

Pore characteristics analysis with μCT

With the μCT, the total volume of interest (VOI), object volume, open porosity and pore connectivity of woods were shown in Tab. 2. The open porosity represented the amount of the valid pores and the pore connectivity was defined as a measure of the degree to which a structure was multiply connected. The void pore volume was 4.44, 2.71 cm^3 for 0.23 and 0.40 g.cm^{-3} samples, respectively. The open porosity and connectivity of 0.23 g.cm^{-3} sample were larger than those of 0.40 g.cm^{-3} sample, and indicated that the 0.23 g.cm^{-3} sample had more valid pores and good connectivity between voids. The open pore size distribution of range from 2.84 to 36.86 μm was provided by the CTAn analysis and shown in Fig. 6. The pore distribution tendencies of the two samples were similar. For a few microns to 10 microns might be pits, wood fiber cell cavity and the pointed ends of vessel lumina, and larger pores could were vessel lumina, wood ray cell lumina. For the 0.23 g.cm^{-3} sample, the pores of 8.51 -36.85 μm were significantly more than that of 0.40 g.cm^{-3} sample (Fig. 5) but 2.84 -8.51 μm pores were less. These results were similar to MIP measurement. (Figs. 2, 3).

Tab. 2: The results of "CT-analysis" for Populus L. woods.

Density ($g.cm^{-3}$)	Total VOI volume (cm^3)	Object volume (cm^3)	Open porosity (%)	Connectivity
0.23	6.94	2.50	63.99031	1625905
0.40	4.72	2.01	57.52574	1010708

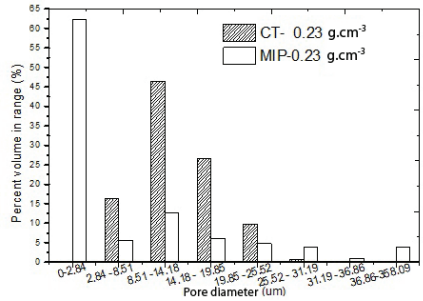

Fig. 6: Pore size distribution of Populus L. *wood by MIP and Micro-CT.*

Fig. 6 shows the pore volume percentage distribution with pore diameter by the μCT and MIP for 0.23 $g.cm^{-3}$ samples. The pore size distributions obtained from the μCT and MIP were 2.84~36.86 μm and 3.1~400 μm, respectively. The overlapping pore-size range of MIP and μCT is schematically visualized on the pore-size distribution in Fig. 6. For the μCT analysis, the smallest pore was determined by the scanning resolution. For example, the pores in the range of 0-2.84 μm were not distinguished. For the MIP, the amount of percent volume of pores for each bin was determined directly from the intrusion mercury volume and pressure. The larger pores percentage for the μCT was more than that of the MIP. This result was in agreement with the observation by Abell et al. (1999). The results of MIP measurement indicated that most pores size were less than 2.84 μm. This outcome might result from the following reasons. First, ink-bottle effect leads to an overestimation of the pits and tiny voids volume and an underestimation of the cell lumen volume (Chen 2012). Second, according to the MIP measurement mechanism, smaller pores need a higher pressure. The extremely high mercury pressure might cause the collapse of nanoscale pores (Burdine 1953). The nanoscale pores could be accurately measured if the scanning resolution of CT has been improved to nano-level in the future development.

CONCLUSIONS

The pore characteristics of *Populus* L. woods were characterized with the MIP and μCT. It was concluded that:

1. As for MIP, the measurement of pore size of Populus L. woods ranged from 50 nm to 400 μm. The pore volume in the range of 313-2513.7 nm and 8-400 μm for 0.23 $g.cm^{-3}$ sample were significantly larger than that for 0.40 $g.cm^{-3}$ sample, but the pore volume in the range of 2513.7-7878 nm was less. However, the measured micro-voids volume ranged from 50 nm to 1 μm was more than actual value due to the ink-bottle pores.
2. As for μCT measurement, the pore distribution tendencies of the two samples were similar. For the 0.23 $g.cm^{-3}$ sample, the pores of 8.51 -36.85 μm were significantly more than the 0.40 $g.cm^{-3}$ sample, but 2.84 -8.51 μm pores were less. The micro-voids were significantly

more than 0.40 g.cm^{-3} samples' resulting in larger hysteresis region.

3. Compared with the results of μCT and MIP, The pore size distributions tendencies were smaller, but the larger pores percentage for the μCT was more than that of the MIP. Moreover, the existence of ink-bottle effect of MIP was confirmed. Ink-bottle effect led to an overestimation of the pits and tiny voids volume and an underestimation of the cell lumen volume.

ACKNOWLEDGMENT

The authors gratefully acknowledge the support of the state forestry administration of China "948 "project (High performance wood-based composite sound absorption material preparation technology import, 2013-4-15).

REFERENCES

1. Abell, A.B., Willis, K.L., Lange, D.A., 1999: Mercury intrusion porosimetry and image analysis of cement-based materials. Journal of Colloid and Interface Science 211(1): 39-44.
2. Burdine, N.T., 1953: Relative permeability calculations from pore size distribution data. Journal of Petroleum Technology 5(03): 7.
3. Chen, Y., 2012: Adsorption performance and characterization of porous materials. In: Preparation and characterization of porous materials (2ed). University of science and technology of China press, China. Pp 15-16.
4. Cnudde, V., Cwirzen, A., Masschaele, B., Jacobs, P., 2009: Porosity and microstructure characterization of building stones and concretes. Engineering geology 103(3): 76-83.
5. Ding, W.D., Koubaa, A., Chaala, A., Belem, T., Krause, C., 2008: Relationship between wood porosity, wood density and methyl methacrylate impregnation rate. Wood Material Science and Engineering 3(1-2): 62-70.
6. Griffin, D.M., 1977: Water potential and wood-decay fungi. Annual Review of Phytopathology 15(1): 319-329.
7. He, S., Lin, L.Y., Fu F., Zhou, Y.D., Fan, M.Z., 2014: Microwave treatment for enhancing the liquid permeability of Chinese fir. BioResources 9(2): 1924-1938.
8. http://www.doc88.com/p-4971074126021.html. pdf. October 15.2014.
9. Mizuno, S., Torizu, R., Sugiyama, J., 2010: Wood identification of a wooden mask using synchrotron X-ray microtomography. Journal of Archaeological Science 37(11): 2842-2845.
10. Moore, M. J., Jabbari, E., Ritman, E.L., Lu, L., Currier, B.L., Yaszemski, M.J., 2004: Quantitative analysis of interconnectivity of porous biodegradable scaffolds with micro-computed tomography. Journal of Biomedical Materials Research Part A 71(2): 258-267.
11. Moro, F., Böhni, H., 2002: Ink-bottle effect in mercury intrusion porosimetry of cement-based materials. Journal of colloid and interface science 246(1): 135-149.
12. Penumadu, D., Dean, J., 2000: Compressibility effect in evaluating the pore-size distribution of kaolin clay using mercury intrusion porosimetry. J. Canadian Geotechnical Journal 37(2): 393-405.
13. Plötze, M., Niemz, P., 2011: Porosity and pore size distribution of different wood types as determined by mercury intrusion porosimetry. Journal of Wood and Wood Products 69(4): 649-657.

14. Roels, S., Elsen, J., Carmeliet, J., Hens, H., 2001: Characterisation of pore structure by combining mercury porosimetry and micrography. Materials and structures 34(2): 76-82.
15. Steppe, K., Cnudde, V., Girard, C., Lemeur, R., Cnudde, J., Jacobs, P., 2004: Use of X-ray computed microtomography for non-invasive determination of wood anatomical characteristics. Journal of structural biology 148(1): 11-21.
16. Suleiman, B.M., Larfeldt, J., Leckner. B., Gustavsson, M., 1999: Thermal conductivity and diffusivity of wood. Wood science and technology 33(6): 465-473.
17. Thygesen, L.G., Engelund, E.T., Hoffmeyer, P., 2010: Water sorption in wood and modified wood at high values of relative humidity. Part I: results for untreated, acetylated, and fur furylated Norway spruce. Holzforschung 64(3): 315-323.
18. Young, T., 1805: An essay on the cohesion of fluids. Philosophical Transactions of the Royal Society of London 95: 65-87.
19. Wang, D., Peng, L.M., Zhu, G.Y., Fu, F., Zhou, Y.D., Song, B.Q., 2014: Improving the sound absorption capacity of wood by microwave treatment. BioResources 9(4): 7504-7518.

Li Min Peng, Dong Wang, Feng Fu, Bo Qi Song*
Research Institute of Wood Industry
Chinese Academy of Forestry
Beijing
China
Phone: +86 010 62889429
Corresponding author: penglm@caf.ac.cn